



## Research paper

## Glucose-functionalized amino-OPEs as biocompatible photosensitizers in PDT



Elisa Deni <sup>a,1</sup>, Alicia Zamarrón <sup>b,1</sup>, Paola Bonaccorsi <sup>a</sup>, M. Carmen Carreño <sup>c</sup>,  
 Ángeles Juarranz <sup>b</sup>, Fausto Puntoriero <sup>a</sup>, Maria Teresa Sciortino <sup>a</sup>,  
 María Ribagorda <sup>c,\*</sup>, Anna Barattucci <sup>a,\*\*</sup>

<sup>a</sup> Dipartimento di Scienze Chimiche, Biologiche, Farmaceutiche ed Ambientali- ChiBioFarAm, Università di Messina, Messina, Italy

<sup>b</sup> Departamento de Biología, Universidad Autónoma de Madrid, Madrid, Spain

<sup>c</sup> Departamento de Química Orgánica, Universidad Autónoma de Madrid, Madrid, Spain

## ARTICLE INFO

## Article history:

Received 10 December 2015

Received in revised form

21 December 2015

Accepted 21 January 2016

Available online 28 January 2016

## Keywords:

Photodynamic therapy

Photosensitizer

Oligo(phenylene ethynylene)

Singlet oxygen production

Glucose base photosensitizers

## ABSTRACT

Photodynamic therapy (PDT) is a minimally invasive procedure that can provide a selective eradication of neoplastic diseases by the combined effect of a photosensitizer, light and oxygen. New amino oligo(phenylene-ethynylene)s (OPEs), bearing hydrophilic glucoside terminations, have been prepared, characterized and tested as photosensitizers in PDT. The effectiveness of these compounds in combination with UVA light has been checked on two tumor cell lines (HEp-2 and HeLa cells, derived from a larynx carcinoma and a cervical carcinoma, respectively). The compounds triggered a mitotic blockage that led to the cell death, being the effect active up to 3  $\mu\text{M}$  concentration. The photophysical properties of OPEs, such as high quantum yield, stability, singlet oxygen production, biocompatibility, easy cell-internalization and very good response even at low concentration, make them promising photosensitizers in the application of PDT.

© 2016 Elsevier Masson SAS. All rights reserved.

## 1. Introduction

Phototherapy is a minimally invasive therapeutic procedure already approved for the treatment of various oncological and non-oncological pathologies of skin [1,2]. Variants of phototherapy include targeted ultraviolet B (UVB) phototherapy, topical psoralen plus ultraviolet A (PUVA), and photodynamic therapy (PDT). All of them are localized forms of phototherapy, either as first-line treatment or as complementary treatment for those that do not

respond to other topical treatments [3,4]. PDT is based on the specific accumulation of a photosensitizer (PS) in the target tissue, followed by irradiation with light at a wavelength matching the absorption spectrum of the PS. Upon light absorption, the PS transits from its ground state to an unstable excited singlet state, from which it can decay, either to the ground-state or to the excited triplet state. In this long-lived excited triplet state, the PS is able to produce singlet oxygen ( $^1\text{O}_2$ ) which, in turn, gives rise to other reactive oxygen species (ROS), such as peroxides, superoxide anions or hydroxyl radicals. Taking into account that  $^1\text{O}_2$  has a lifetime of approximately 40 ns, it acts near to the site where it is generated. ROS are able to react directly with a biological substrate, oxidizing vital cellular components inducing an acute cell stress response culminating in cellular death, mainly by apoptosis and/or necrosis. The cell death pathway depends, among other factors, on the nature and intracellular localization of the PS and on tumor properties [1,5].

Due to their selectivity towards tumor tissue in PDT, porphyrins and porphyrin-related macrocycles are at the forefront of PDT [6]. Several compounds belonging to a first generation of PSs, such as the hematoporphyrin derivative HpD (Photofrin) [1,5], are already

*Abbreviations:* OPE, oligo(phenylene ethynylene); PDT, photodynamic therapy; PS, photosensitizer; UV, ultraviolet light; UVA, ultraviolet light A; UVB, ultraviolet light B; PUVA, psoralen plus ultraviolet A therapy; ROS, reactive oxygen species; LD50, lethal dose 50%; LD90, lethal dose 90%; MTT, 3-[4,5-dimethylthiazol-2-yl]-2,5-diphenyltetrazolium bromide; AO-EtBr, acridine orange-ethidium bromide; MTs, microtubules.

\* Corresponding author.

\*\* Corresponding author. Dipartimento di Scienze Chimiche, Biologiche, Farmaceutiche ed Ambientali- ChiBioFarAm, Università di Messina, Messina, Italy.

E-mail addresses: [maria.ribagorda@uam.es](mailto:maria.ribagorda@uam.es) (M. Ribagorda), [abarattucci@unime.it](mailto:abarattucci@unime.it) (A. Barattucci).

<sup>1</sup> The first and second authors contributed equally to this work.

in clinical use or in clinical trials to treat cancer patients and are approved by the Food and Drug Administration for the palliative treatment of obstructive lung and esophageal cancers. A second-generation of PSs, with improved pharmacokinetics and reduced skin photosensitivity, includes aminolevulinic acid (ALA; a pro-PS), widely used for the treatment of non melanoma skin cancer (NMSC), benzoporphyrin derivative (BPD), silicon phthalocyanine (Pc4) or *m*-tetrahydroxyphenylchlorin (mTHPC) [1,2]. In the case of PUVA, psoralens are excited by UVA light at suberythemogenic doses and have been used to treat determined skin diseases, including psoriasis, vitiligo and mycosis fungoides [7–9].

Photosensitizers based on amphiphilic skeletons, bearing lipophilic and hydrophilic moieties, are in continuous development due to their biological applications. For instance, symmetric and asymmetrically substituted phthalocyanines bearing hydrophilic D-galactose units have shown to be efficient PSs towards HeLa cells [10], while glucose-appended Iron(III) complexes caused HeLa cells apoptosis by the generation of ROS on irradiation [11].

The ideal photosensitizers [12] should possess high photoactivity and selective photocytotoxicity for sick skin cells but low dark toxicity, activation at discrete wavelengths, efficient and fast distribution and elimination from tissues and chemical and physical stability. Although a significant number of PS are synthesized each year, the development of new targets that fulfill all the requirements continues to be an appealing area of research in phototherapy [13]. Oligo(phenylene-ethynylene)s (OPEs) are luminescent linear oligomers with extended conjugated aromatic and ethynylene moieties. Due to their intriguing optical and electronic properties [14], OPEs have lately gained a prominent role in the design of organic materials such as sensing or electronic organic devices. On the other hand, there are only few examples of their use in biological fields. For instance, OPEs incorporating cationic ends have been shown to behave as light-activated biocides, killing some specific kind of bacteria, as a result of the production of singlet oxygen after irradiation [15]. Galactose-functionalized oligomers have been shown to act as inhibitors of *Pseudomonas aeruginosa* lectin LecA [16]. *N*-Hydroxy succinimidoyl esters incorporated to OPEs were reported to behave as luminescent labeling probes for proteins [17]. Aryleneethynylene compound bearing two polar sulfonate groups has been reported as effective fluorescent markers for liposomes and mammalian cell membranes [18]. In spite of the encouraging electronic properties displayed by the OPEs, to our knowledge, there are no precedents of their use as photosensitizers in photodynamic therapy.

Following our biological studies of carbohydrate based conjugated systems [19–21], we recently prepared several end-glucose functionalized OPEs and reported their ability to permeate the cellular cancer membrane and to localize in cytoplasmic organelles [22]. Few structural features were found to be crucial to reach an efficient cytoplasmatic OPE dye: three aryl ethenyl conjugated units, two hydrophilic glucose molecules at both ends of the OPE skeleton and, a dimethylamino substituent at the central aryl ring of the conjugated system (see compound **1** in Fig. 1). Preliminary biological evaluation tests demonstrated that these OPE derivatives were non-cytotoxic. Taking into account these precedents, we decided to study the behavior of two OPE derivatives, as biocompatible photosensitizers targets in PDT (Fig. 1). Herein we report full details of the preparation of end-glucose OPE derivative **1** and a new derivative **2**, the photophysical studies and *in vitro* toxicity, either in the absence of light or under light irradiation, against HeLa and HEp-2 tumor cell lines. The presence of hydrophobic (aryl conjugated fragments) and hydrophilic (glucose) moieties in these structures was expected to facilitate cellular membrane permeation. Moreover, the terminal glucose molecules were chosen considering the enhanced glycolytic process of cancer

carbohydrate metabolism (Warburg effect) [23].

## 2. Results and discussion

### 2.1. Chemistry

The target dimethylamino-derived OPE glucosides **1** and **2**, having one or two *N,N*-dimethylamino substituted aryl moieties respectively, are depicted in Fig. 1.

The synthesis of compound **1** was completed following a strategy previously reported by us [22], based on copper-free Sonogashira type coupling to assemble the triple bonds to the adequately substituted aromatic rings, in a convergent manner (Scheme 1). Thus, compound **1** was prepared from the key intermediate *N,N*-dimethyl-2,5-bis[(trimethylsilyl)ethynyl] aniline **4**, which allowed a double Pd(0) catalyzed cross-coupling reaction with iodo aryl derivative **7**, incorporating the 2,5-dimethoxy aryl substituents as well as the acetylated glucoside methylene ethynyl moiety, leading to the final carbon skeleton in one step. Precursor **4** was prepared in 55% isolated yield, using a Pd(0) cross-coupling reaction between *N,N*-dimethyl-2,5-dibromoaniline **3** and an excess of ethynyl-trimethylsilane, whereas compound **7** was efficiently formed by Pd mediated cross-coupling of 1,4-diiodo-2,5-dimethoxybenzene **5** [24] and tetraacetylpropynyl glucoside **6** [25]. The use of 2 equivalents of the diiododerivative **5** was essential to achieve a high yield for the preparation of **7**. Inspired by the work of Mori [26], and Naso [27] we successfully achieved the cross-coupling reaction between **4** and **7** (2 equiv) in 61% yield using [Pd(PPh<sub>3</sub>)<sub>4</sub>] as catalyst in the presence of Ag<sub>2</sub>O, which was known to act as activator facilitating coupling between aromatic iodides and silane derivatives. Final deprotection of acetylated glucoside moieties gave the desired gluco-OPE **1**.

Preparation of gluco-OPE **2** is based on a convergent strategy that allows a double assembly of a gluco-2-propynyl aryl ethynylene framework with the aryl central core 1,4-diiodo-2,5-dimethoxy benzene **5** (Scheme 2). It is noteworthy to mention that the Pd(0) mediated coupling reaction of **6** and 2,5-dibromo aryl derivative **3**, [28] in an appropriate molecular ratio (1:1), exclusively led to the mono substituted regioisomer **8**, [29] resulting from reaction on the less sterically hindered 5-bromo substituent situated *meta* to the bulky dimethylamino group of **3**, in a 60% yield. The palladium catalyzed cross-coupling reaction between **8** and an excess of commercially available trimethylsilylacetylene gave rise to the key intermediate **9** in high yield under very mild conditions. The final Ag<sub>2</sub>O-modified Pd(0) mediated coupling [26,27] between **9** (2 equiv) and 1,4-diiodo-2,5-dimethoxy benzene **5** allowed a double assembly that directly lead to the desired carbon skeleton of OPE **10**. All the newly synthesized intermediates **8**, **9** and **10** could be purified by conventional flash column chromatography and are stable and easy to handle. Finally, quantitative deacetylation of **10** in the presence of an excess of aqueous ammonia gave the gluco-OPE **2** as a brilliant yellow solid, easily separated from residual acetamide by subsequent washings with MeOH, in almost quantitative yield.

### 2.2. Photophysical properties

The absorption and photophysical data of the final OPE glucosides **1** and **2** in aqueous solution are summarized in Table 1. For comparison purposes, the data of all 2,5-dimethoxy aryl ring gluco-OPE **11** [22] (Fig. 2), previously studied by us are also included.

The absorption spectra of the OPEs **1** and **2**, in aqueous solution (pH = 7.2, buffer phosphate, see Fig. 3), are characterized by intense broad low-energy absorption bands centered at 388 nm and at 392 nm, respectively with  $\epsilon$  values in the range  $10^4$ – $10^5$  M<sup>-1</sup> cm<sup>-1</sup>.

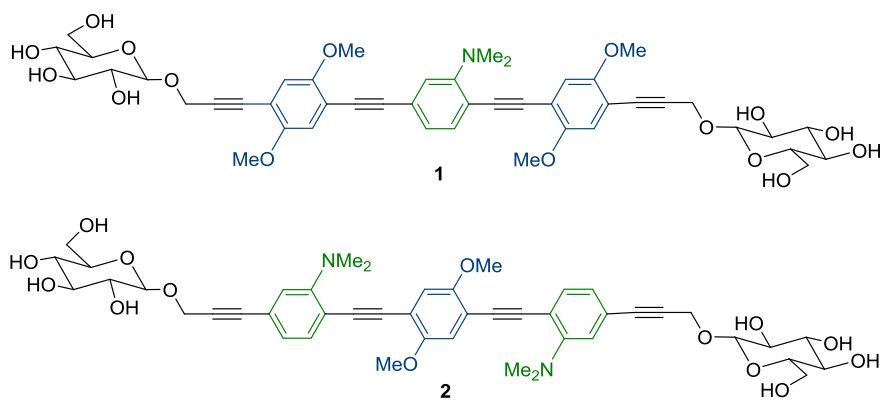
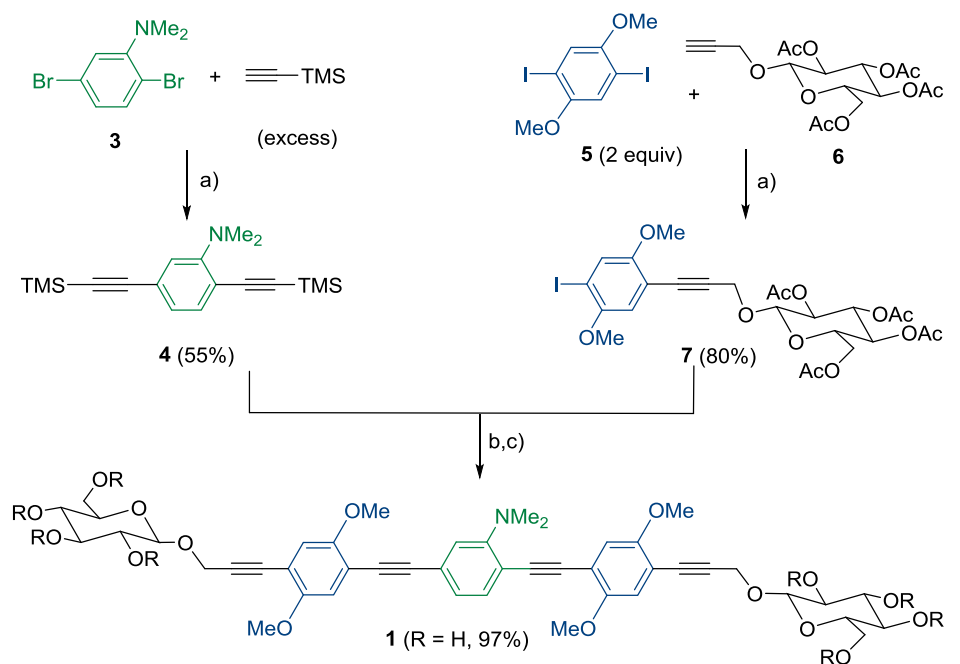


Fig. 1. Structure of gluco-OPEs 1 and 2.



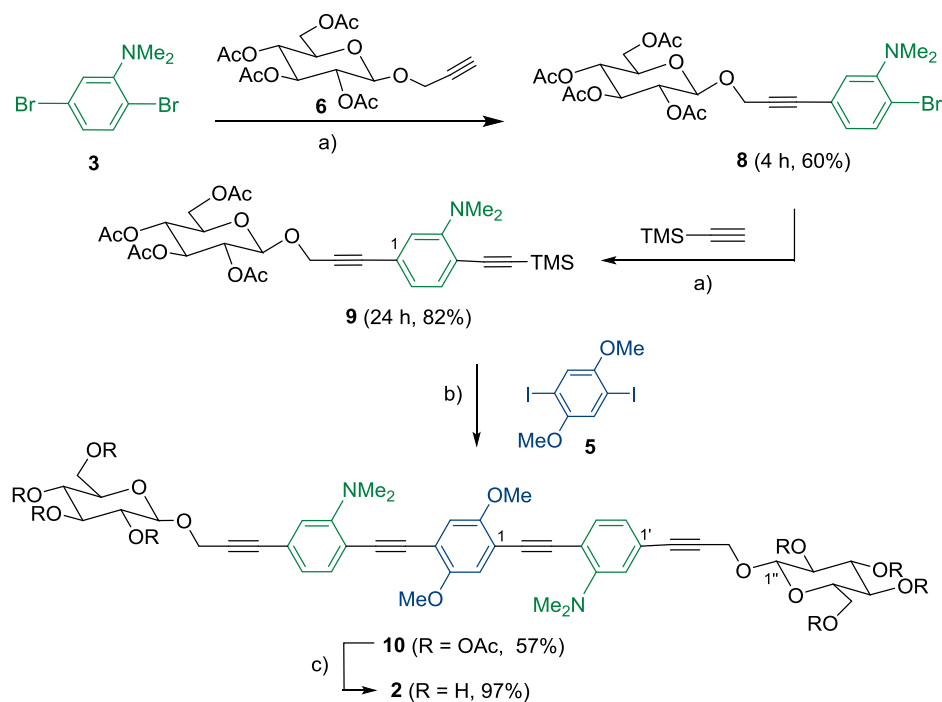
a)  $[\text{Pd}(\text{PPh}_3)_4]$ ,  $\text{NEt}_3$ , DMF,  $65^\circ\text{C}$ , 2 h; b)  $[\text{Pd}(\text{PPh}_3)_4]$ ,  $\text{Ag}_2\text{O}$ , DMF/THF,  $70^\circ\text{C}$ , 7 h,  $\text{R} = \text{Ac}$ , 61%; c)  $\text{NH}_4\text{OH}$ , THF/MeOH, RT, 16 h.

Scheme 1. Synthesis of gluco-OPE 1.

According with literature [30], these absorptions in the UV region are due to spin-allowed  $\pi-\pi^*$  transitions and are attributed to Internal Charge Transfer (ICT) transitions. The excitation of compounds **1** and **2** in the range of 280–420 nm allowed the appearance of emission bands in the blue region of spectrum. Interestingly, the results presented in Table 1 revealed clear differences between the photophysical properties of **1** and **2**. In particular, moving from **1** to **2**, the emission quantum yield increased, from  $\Phi = 0.57$  (**1**) to  $\Phi = 0.74$  (**2**), as well as the excited state lifetime, from  $\tau/\text{ns} = 2.47$  (**1**) to  $\tau/\text{ns} = 3.54$  (**2**). Remarkably, both quantum yields were reduced with respect to the analogous model compound **11** ( $\Phi = 0.85$ ) in which no dimethylamino group is present. This behavior could suggest that the excited singlet states decay faster in **1** because, in this case, the rate of inter-system crossing to the triplet excited state (responsible for sensing singlet oxygen) is enhanced with respect to **2** and **11**.

On the basis of this assumption, we performed an indirect

evaluation of singlet oxygen production by excitation of the oligomers **1**, **2** and **11**. The singlet-oxygen generation was evaluated by a chemical method using uric acid (UA) as detector and the methylene blue species as a reference photosensitizer [31,32]. Under irradiation, at neutral pH, uric acid is stable and shows one absorption band centered at 292 nm. When singlet oxygen (or ROS) is photo-produced, uric acid is irreversibly oxidized as highlighted by the reduced intensity of its absorption band. The decay curves of the UA absorption band ( $\lambda_{\text{max}} 292 \text{ nm}$ ) as a function of the irradiation time in the presence of **1**, **2** and the model **11** are reported in Fig. 4. A strong decay was observed upon irradiation of the uric acid solution in the presence of OPE-**1** at 380 nm, and a moderate decay was observed in the presence of OPE-**2** upon irradiation at 390 nm. On the contrary, the UA absorption band remained unchanged upon irradiation at 380 nm in the presence of OPE-**11**. These photophysical results are in agreement with the singlet oxygen quantum yields previously obtained for **1** ( $\Phi_{1\text{O}_2} 0.15$ ) and **2** ( $\Phi_{1\text{O}_2} 0.09$ )



a)  $[\text{Pd}(\text{PPh}_3)_4]$ ,  $\text{NEt}_3$ , DMF, 65 °C; b)  $[\text{Pd}(\text{PPh}_3)_4]$ ,  $\text{Ag}_2\text{O}$ , DMF/THF, 70 °C, 7 h; c)  $\text{NH}_4\text{OH}$ , THF/MeOH, RT, 16 h.

**Scheme 2.** Synthesis of gluco-OPE 2.

**Table 1**  
Spectroscopic and photophysical data of **1**, **2** and **11** in buffered aqueous solution.<sup>a</sup>

OPEs	Absorption $\lambda_{\text{max}}$ nm ( $\epsilon/\text{M}^{-1} \text{cm}^{-1}$ ) <sup>b</sup>	Luminescence at 298 K			
		$\lambda_{\text{max}}$ nm	$\Phi$	$\tau/\text{ns}$	$\Phi_{1\text{O}_2}$
<b>1</b>	388 (38900)	472	0.57	2.47	0.15
<b>2</b>	392 (40000)	474	0.74	3.54	0.09
<b>11</b> <sup>c</sup>	390 (49500)	433 <sup>c</sup>	0.85 <sup>c</sup>	0.98 <sup>c</sup>	–

<sup>a</sup> Buffer phosphate aqueous solution, pH = 7.2.

<sup>b</sup> For the absorption, the maxima or shoulders of the lower energy bands are given.

<sup>c</sup> Data from Ref. [22].

(see Table 1), confirming that the reduced luminescence quantum yield for **1** could be ascribed to a more efficient sensitization of the triplet excited state of these species.

### 2.3. Biological study. Subcellular localization of PSs

The efficiency of a photosensitizer for PDT is related to its subcellular localization [33,34]. Therefore, we first evaluated the cell internalization and localization of OPE compounds **1** and **2**. The subcellular localization of **1** and **2** in HaCaT, HeLa and HEP-2 cells was analyzed by fluorescence microscopy under UV excitation light (360–370 nm) (Fig. 5A). Similar results were observed under blue light excitation (460–490 nm) (Fig. S15, ESI). The intracellular luminescent signals of **1** and **2** were observed after 6 h of incubation with  $1 \cdot 10^{-6}$  M of both compounds. Corresponding controls (without PSs incubation) of each cell type were also performed. In the three cell lines, after the incubation with PSs, an intense signal was visualized around the nucleus in a reticular pattern, as well as in a yuxtannuclear position. By contrast, control cells showed a very low signal, corresponding to mitochondrial autofluorescence. This

indicated that signal emitted by treated HaCaT, HeLa and HEP-2 cells was due to the intracellular accumulation of the PSs, confirming the cellular uptakes of both compounds. In order to determine the places where PSs were located, cells were incubated with known markers for endoplasmic reticulum (ER-Tracker<sup>®</sup>) and Golgi apparatus (NBD<sup>®</sup>) (Fig. 5B). Comparison of the images obtained after incubation with **1** and **2** with those obtained with the known probes for specific organelles, confirmed that compounds **1** and **2** are localized mainly in Golgi apparatus and endoplasmic reticulum. It is important to indicate that no differences were found in the intracellular localization of OPE-1 or 2 in the three cell types.

### 2.4. Effects induced by 1 and 2 – PDT on cell survival

The action of a PS on cells is related to the production of  $^1\text{O}_2$  and/or other ROS generated after light irradiation [1,15,35]. Therefore, we next evaluated the toxicity of compounds **1** and **2** first in the absence of light and then after UV irradiation. The toxicity experiments were performed by incubation of HaCaT, HeLa or HEP-2 cells with **1** or **2** (ranging from  $3 \cdot 10^{-6}$  to  $2.5 \cdot 10^{-5}$  M) in the dark. In the absence of light the toxicity for both OPEs **1** and **2**, was dependent on the PS concentration (Table 2). Thus, concentrations of  $3 \cdot 10^{-6}$  and  $5 \cdot 10^{-6}$  M of both PSs did not induce any relevant toxic effect (survival rates above 90% in all cell lines), and higher PS concentrations ( $1 \cdot 10^{-5}$  and  $2.5 \cdot 10^{-5}$  M) caused a variable cell damage depending on the cell type (survival percentages between 60 and 85%). The dark toxicity levels obtained for both OPEs **1** and **2** are similar to other reported PSs tested *in vitro*, including porphyrin derivatives and phthalocyanines [36,37].

We next evaluated the effect of UVA irradiation on the cell cultures, first without the presence of the OPEs. As can be seen in Table 3, none of the tested doses (ranging from 0.25 to 2 J/cm<sup>2</sup>) induced substantial cytotoxic effects, the survival rates of HaCaT, HeLa and HEP-2 after UVA light irradiation (2 J/cm<sup>2</sup>) were 97.2%,

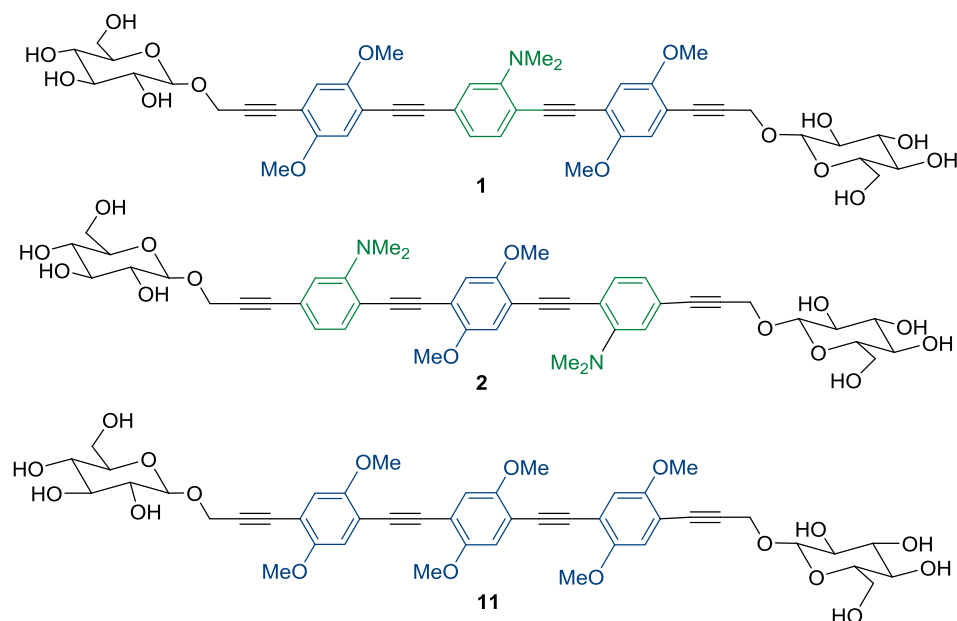


Fig. 2. Structure of gluco-OPEs **1**, **2** and **11**.

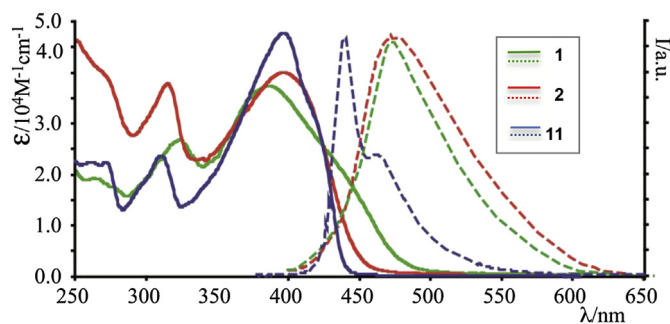


Fig. 3. Absorption (solid line) and emission (dotted line) spectra of **1** (green), **2** (red) and **11** (blue) in aqueous phosphate buffered solution, pH = 7.2. (For interpretation of the references to colour in this figure legend, the reader is referred to the web version of this article.)

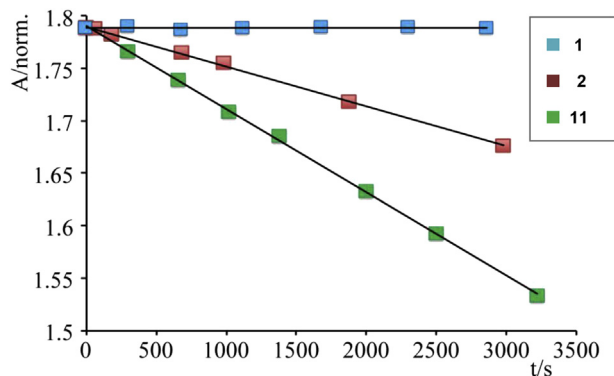


Fig. 4. Degradation of uric acid ( $\lambda_{\max} = 292$  nm) versus Time using as sensitizer OPE-1 (green squares,  $5 \cdot 10^{-5}$  M) irradiated at 380 nm, OPE-2 (red squares,  $5 \cdot 10^{-5}$  M) irradiated at 390 nm and the model OPE-11 (blue squares,  $5 \cdot 10^{-5}$  M) irradiated at 380 nm. (For interpretation of the references to colour in this figure legend, the reader is referred to the web version of this article.)

94.0% and 95.1%, respectively.

According to the above results we selected concentrations of

$3 \cdot 10^{-6}$  and  $5 \cdot 10^{-6}$  M of both compounds and 0.25, 0.5 and 1 J/cm<sup>2</sup> of UVA light to evaluate the synergic effect of the PSs compounds **1** and **2** plus UVA irradiation on the three cell lines. The photodynamic treatments, carried out by incubation with OPE-1 or OPE-2 for 6 h followed by UVA exposure, induced cytotoxic effects in HaCaT, HeLa and HEp-2, depending on the PS concentration and the UVA dose. Cell survival rates after PDT (Fig. 6A), measured by MTT assay, were significantly decreased ( $P < 0.01$ ) in all the cell lines with respect to untreated controls. Viability after PDT were similar for both PSs, since no significant differences between **1** and **2** were found. However, HeLa cells tended to be slightly more sensitive to PDT than HaCaT and HEp-2. The LD50 dose (treatment conditions that induced approximately a 50% of cell death) was reached with concentrations of  $3 \cdot 10^{-6}$  of **1** or **2** followed by 0.25 J/cm<sup>2</sup> of UVA radiation. The other tested conditions caused a lethality rate greater than 50%. In the case of **1**, values lower than 10% of cell survival (LD90) were obtained after cell treatment with  $2.5 \cdot 10^{-5}$  M and 2 J/cm<sup>2</sup> of UVA light (Fig. S16, ESI); similar results were found for **2**. All these findings indicated that compounds **1** and **2** were not toxic for the cells in the absence of light at concentrations lower than  $5 \cdot 10^{-6}$  M, confirming that the cytotoxic effect when UVA light was applied was due to the production of reactive oxygen species. These cytotoxic values are comparable with other PSs used in PDT under UVA light irradiation, such as curcumin [38], hypericin or psoralen [39]. Both PSs reached a good photodynamic effect when combined with UVA light, but we did not observe selectively for tumor HeLa and HEp-2 cells compared to non-tumor HaCaT cell line.

The cell morphology was also analyzed 24 h after phototreatments, using phase contrast microscopy (Fig. 6B). This analysis revealed that **1** and **2**-based PDT induced notable changes in the morphology of HaCaT, HeLa and HEp-2 cells. These alterations were dependent on the treatment conditions (PS concentration and UVA light dose) and did not differ when **1** or **2** were used. Under a LD50 conditions, HaCaT cells showed cytoplasmic retraction and cell elongation, as well as the appearance of apoptotic (with membrane blebbing) and necrotic (with loss of membrane integrity) figures. The tumoral cell lines (HeLa and HEp-2) also suffered retraction of their cytoplasm, cellular stretching and a strongly cytoplasmic vacuolization, which is indicative of cell degeneration processes. In addition, we noticed the apparition of a large amount of rounded

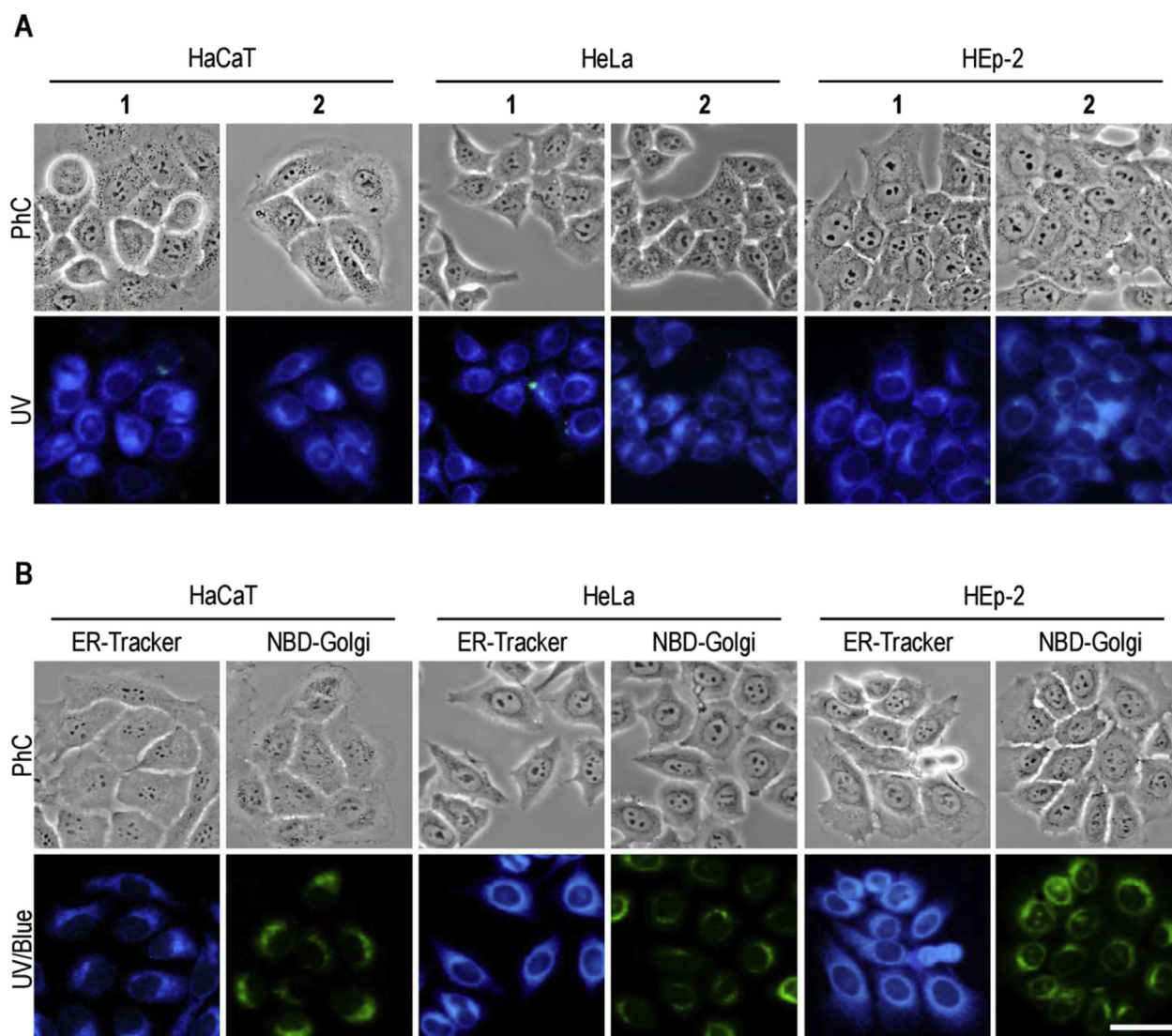


**Fig. 5.** (A) Subcellular localization of OPE-1 and OPE-2 in HaCaT, HeLa and Hep-2 cells. After 6 h of incubation with  $1 \cdot 10^{-6}$  M of PSs, a blue fluorescence was observed under UV excitation light. This fluorescence had a reticular distribution and also appeared in a yuxtannuclear position. (B) Intracellular localization of ER and Golgi apparatus in HaCaT, HeLa and Hep-2 cells. Cells were incubated with known markers for endoplasmic reticulum (ER-Tracker) and Golgi apparatus (NBD-Golgi). ER showed a blue fluorescent signal under UV excitation light ( $\lambda = 360\text{--}370$  nm) and Golgi apparatus emitted a green fluorescence under blue excitation light ( $\lambda = 460\text{--}490$  nm). Scale bar: 20  $\mu\text{m}$ . (For interpretation of the references to colour in this figure legend, the reader is referred to the web version of this article.)

**Table 2**

Dark toxicity: Cell survival percentage after incubation with compounds 1 and 2 in the absence of light.<sup>a</sup>

[PS]	HaCaT		HeLa		HEp-2	
	1	2	1	2	1	2
$3 \cdot 10^{-6}$ M	92.36 $\pm$ 1.6	91.45 $\pm$ 1.3	96.38 $\pm$ 1.6	96.61 $\pm$ 2.9	97.22 $\pm$ 1.4	97.73 $\pm$ 1.0
$5 \cdot 10^{-6}$ M	91.41 $\pm$ 2.4	90.93 $\pm$ 2.0	95.43 $\pm$ 1.7	93.52 $\pm$ 2.2	96.28 $\pm$ 2.0	95.72 $\pm$ 2.4
$1 \cdot 10^{-5}$ M	71.55 $\pm$ 3.2	70.23 $\pm$ 2.7	82.21 $\pm$ 2.5	76.89 $\pm$ 3.0	85.63 $\pm$ 2.9	80.07 $\pm$ 2.8
$2.5 \cdot 10^{-5}$ M	61.18 $\pm$ 1.8	59.72 $\pm$ 2.8	77.76 $\pm$ 2.7	66.65 $\pm$ 3.1	81.49 $\pm$ 1.9	70.19 $\pm$ 1.2

<sup>a</sup> Cells were incubated with  $3 \cdot 10^{-6}$ ,  $5 \cdot 10^{-6}$ ,  $1 \cdot 10^{-5}$  and  $2.5 \cdot 10^{-5}$  M of 1 or 2 for 6 h in the dark. Cell survival was evaluated after 24 h by MTT assay.

cells, indicating a possible mitotic blockage, as well as a large number of cells detached from the substrate, floating on culture medium. All the changes observed confirm the results obtained from cell viability assays.

When the treatment conditions induced a 90% of cell death (LD90), deep deformations of cell membrane were seen with both PSs and in the three types of cells analyzed (Fig. S16, ESI).

Nuclear morphology was also evaluated 24 h after PDT by H $\ddot{o}$ chst-33258 staining and fluorescence microscopy (Fig. 7A–B). A nuclear retraction was observed in the three cell lines when subjected to LD50 dose of both phototreatments, in comparison to untreated cells, as well as the appearance of apoptotic and necrotic morphologies. Furthermore, a great amount of mitotic nuclei was observed in HeLa and HEp-2 cell lines, most of them abnormal

**Table 3**  
Cell survival percentage after UVA light irradiation.<sup>a</sup>

UVA dose	HaCaT	HeLa	HEp-2
0.25 J/cm <sup>2</sup>	98.76 ± 1.0	99.01 ± 0.9	98.11 ± 1.8
0.5 J/cm <sup>2</sup>	98.33 ± 1.1	97.50 ± 2.0	98.42 ± 1.3
1 J/cm <sup>2</sup>	97.92 ± 2.1	96.79 ± 1.7	97.33 ± 1.5
2 J/cm <sup>2</sup>	97.2 ± 1.2	94.0 ± 2.3	95.2 ± 1.6

<sup>a</sup> Cells were exposed to UVA light at the indicated doses (0.25, 0.5, 1 and 2 J/cm<sup>2</sup>). Cell survival was evaluated 24 h after irradiation by MTT assay.

metaphases.

### 2.5. Acridine orange/ethidium bromide staining

The cytotoxicity of LD50 of **1** and **2** in PDT was also evaluated *in vivo* using acridine orange/ethidium bromide staining (AO/EtBr) (Fig. 8). This method allowed us to distinguish between viable, rounded, apoptotic and necrotic cells (Fig. S17, ESI). As shown in Fig. 8A, the PDT induced evident alterations in the morphology of HaCaT, HeLa and HEp-2 cells, in comparison with their control counterparts. These morphological changes were similar for both PSs. After PDT, HaCaT cultures showed an increase of apoptotic and necrotic cells. In HeLa and HEp-2 cultures, besides apoptotic and necrotic figures, a large number of rounded cells densely stained as green, were observed. In order to determine the exact percentage of each cellular condition, a cell counting was performed. The percentage of cells in each established condition was similar for **1** (Fig. 8B) and **2** (Fig. 8C) phototreatments. HaCaT cells showed a significant higher proportion of apoptotic and necrotic figures in comparison with tumoral cell lines. By contrast, in the case of HeLa and HEp-2, cell counting revealed a significant increase ( $P < 0.01$ ) of rounded cells as compared to HaCaT and to its control counterparts. All of these results suggest that photodynamic treatment could be triggering a mitotic blockage in tumoral cell lines, while in HaCaT mainly induce apoptotic processes.

### 2.6. Cytoskeleton of microtubules as a target for 1 or 2-PDT

To get insight into the mechanisms by which PDT using **1** or **2** as PSs reach their effects on HaCaT, HeLa and HEp-2 cells, we also evaluated the changes induced by PDT in the cytoskeleton of microtubules (MTs) (Fig. 9). MTs are cytoskeletal polymers essential for cell structure, cell division and intracellular transport and their role in tumor progression makes them a key target for anti-cancer therapies, including PDT [12,40,41]. As shown in Fig. 9A, the interphasic HaCaT, HeLa and HEp-2 cells showed a well-developed MT network and no alterations were observed in the mitotic spindle of dividing cells. However, cells showed a clear increase in microtubular changes 24 h after phototreatments with LD50 doses. Most HaCaT cells retracted their cytoplasm and thus showed an altered and disorganized MT network. Moreover, apoptotic morphologies were also observed. With respect to HeLa and HEp-2 cells, in addition to the described alterations, there was also an increase in the number of dividing cells and many of them showed modifications of the spindle apparatus, such as the presence of extrapoles (three and four-poles spindles) and the consequent abnormalities in the distribution of chromosomes in the metaphase plate.

In order to determine the percentage of cells in possible mitotic blockage, mitotic index was quantified 24 h after **1** and **2** phototreatments (Fig. 9B). As shown in Fig. 9, after **1** and **2**-PDT in LD50 conditions, mitotic index of HeLa and HEp-2 was significantly higher as compared to untreated (control) cells. By contrast, mitotic index of HaCaT cells did not change after PDT. The percentage of

mitotic cells with abnormal metaphase plates was also calculated (Fig. 9B). In the same way, PDT of HeLa and HEp-2 cells subjected to LD50 of **1** or **2** presented a significantly higher percentage of altered metaphases in comparison with untreated cells, while phototreatments did not induce aberrant metaphases in HaCaT cells.

These findings suggest that MTs could be a target of phototreatments with compounds **1** and **2** plus UVA light, which cause the disorganization and collapse of MTs network and, in the case of tumoral cell lines, also the incorrect functioning of mitotic apparatus and thus the appearance of aberrant metaphases.

## 3. Conclusions

In summary, we have prepared two dimethylamino (NMe<sub>2</sub>) aryl substituted OPE glucosides **1** and **2**, by an efficient Pd(0) catalyzed cross-coupling reaction in the presence of Ag<sub>2</sub>O, as a key step. OPE glucosides **1** and **2** have been studied from the photophysical and biological point of view, and have been tested as photosensitizers in photodynamic therapy. These compounds have shown to be highly luminescent and bio-compatible. A good dark toxicity were measured for OPE-**1** and **2** in the range of known PSs such as porphyrin and phthalocyanine derivatives. Compounds **1** and **2** are susceptible to be excited by UVA light and produced a high photodynamic effect causing tumoral cell death even with low singlet oxygen production. This photodynamic effect seems to induce damage in the MTs network of tumoral cells, triggering a blockage in the metaphase of cell cycle, which can lead to cell death. The glucose-ends OPE tested have been able to produce singlet oxygen with moderated efficiencies. The study presented here provides the first use of OPEs as photosensitizers and could be a starting point to extend the application of these luminescent oligomers in photodynamic therapy.

## 4. Experimental section

### 4.1. General synthetic methods

Solvents were purified according to standard procedures. All of the reactions were monitored by TLC on commercially available precoated plates (silica gel 60 F254), and the products were visualized with vanillin [1 g dissolved in MeOH (60 mL) and conc. H<sub>2</sub>SO<sub>4</sub> (0.6 mL)] and UV lamp. Silica gel 60 was used for column chromatography. Proton (<sup>1</sup>H) and carbon (<sup>13</sup>C) NMR spectra were recorded on a Varian 500 spectrometer (at 500 MHz for <sup>1</sup>H; and 125 MHz for <sup>13</sup>C) or a AV-300 Bruker (at 300 MHz for <sup>1</sup>H; and 75 MHz for <sup>13</sup>C) using CDCl<sub>3</sub> as solvent, unless differently stated. Chemical shifts are given in parts per million (ppm) ( $\delta$  relative to residual solvent peak for <sup>1</sup>H and <sup>13</sup>C), coupling constants ( $J$ ) are given in hertz, and the attributions are supported by heteronuclear single-quantum coherence (HSQC), Heteronuclear Multiple Bond Correlation (HMBC) and correlation spectroscopy (COSY) experiments. Chemical shifts are reported in ppm relative to CDCl<sub>3</sub> ( $\delta$  7.26 ppm). For simplification purpose, assigned <sup>1</sup>H and <sup>13</sup>C NMR signals follow the numeration depicted in Scheme 2 (see also ESI). Mass spectra ( $m/z$ ) and HRMS were recorded under the conditions of electron impact (EI) and electrospray (ES) in a Waters VG Autospect spectrometer. Melting points were obtained in open capillary tubes and are uncorrected. Tested compounds **1** and **2** were  $\geq 95\%$  pure as determined by qNMR analysis (see ESI), on Varian 500 spectrometer, according to the quantification protocol described by Henderson [42].

#### 4.1.1. 3-[4-Bromo-3-(dimethylamino)phenyl]-2-propyn-1-yl- $\beta$ -D-glucopyranoside-2,3,4,6-tetraacetate (**8**)

To a flask were added Pd(PPh<sub>3</sub>)<sub>4</sub> (0.45 g, 0.39 mmol, 0.15 equiv),

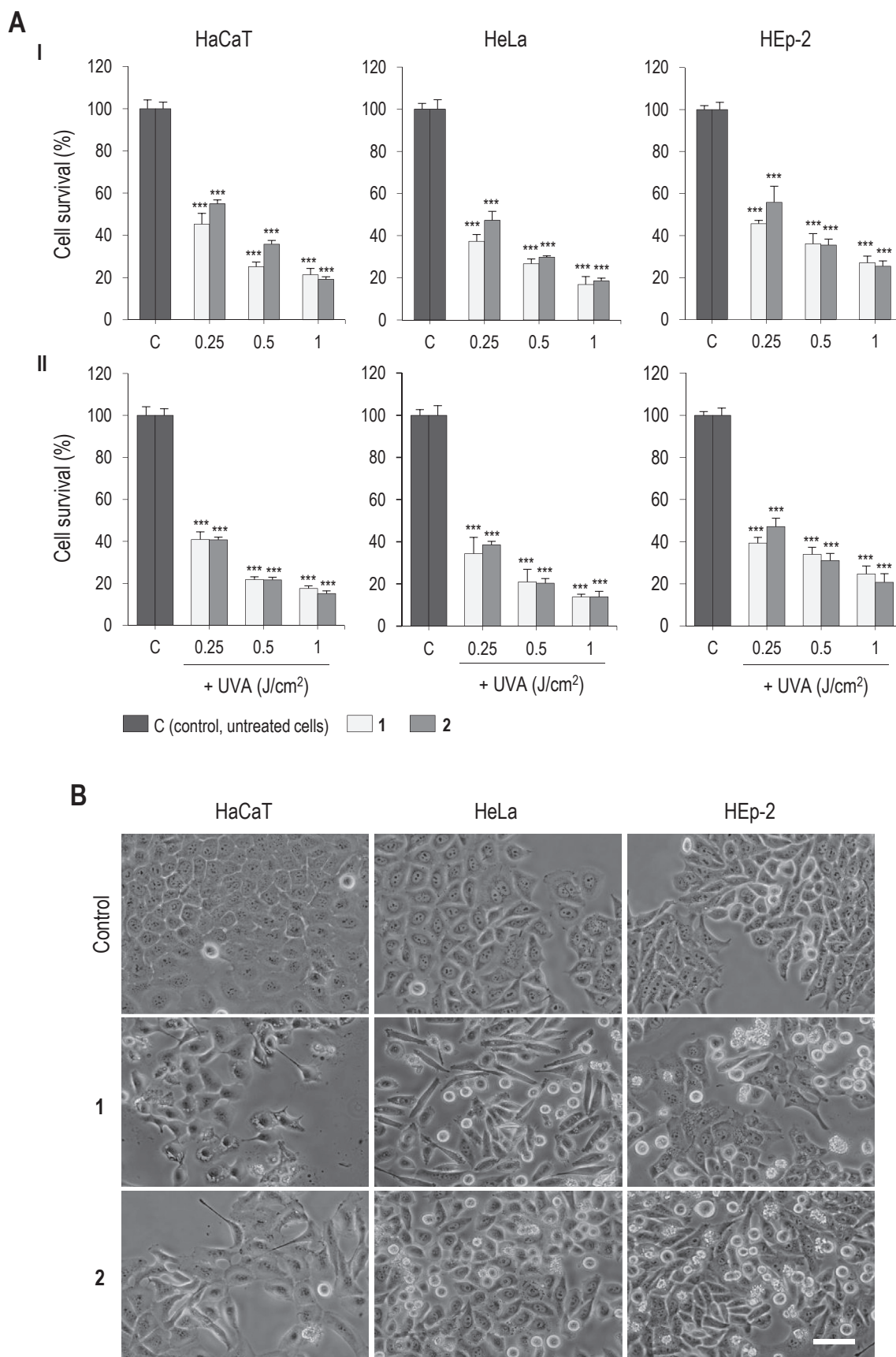


**Fig. 6.** Cell survival rates (**A**) and morphological changes (**B**) after OPE-1 and OPE-2 based PDT. I:  $3 \times 10^{-6}$  M of PSs. II:  $5 \times 10^{-6}$  M of PSs. (**A**) Both 1 and 2-PDT, in all of the treatment conditions applied, caused a significant decrease in HaCaT, HeLa and HEp-2 survival with respect to untreated controls ( $P < 0.01$ ). No significant differences were found between 1

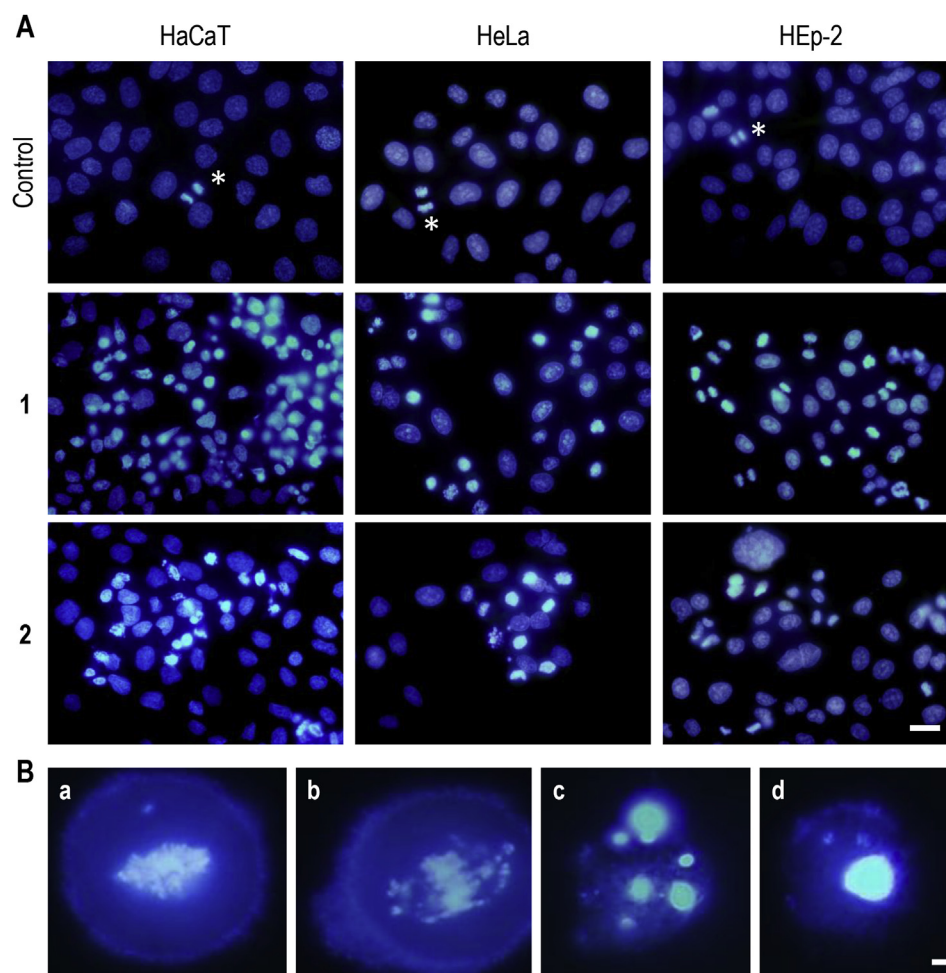


**Fig. 7.** Effect of phototreatments in the nuclear morphology of HaCat, HeLa and Hep-2 cells. Nuclei morphology was observed 24 h after PDT using H $\ddot{o}$ chst-33258 staining and fluorescence microscopy (**A**). The controls (untreated cells) of the three cell lines displayed well defined interphasic and mitotic (\*) nuclei. Nevertheless, when treated with OPE-1 or OPE-2 PDT (LD50 dose), cultures showed an increment of apoptotic and necrotic nuclei. Also, in HeLa and HEp-2 cultures an increase of mitotic cells was observed. (**B**) Details of normal (a) and altered (b) mitotic figures, as well as apoptotic (c) and necrotic (d) cells. Morphologies corresponding to abnormal mitosis, apoptosis and necrosis were found in treated cell cultures, both in cells attached to the substrate and cells detached from it.

**6** (1.00 g, 2.59 mmol, 1 equiv) and **3** (1.45 g, 5.18 mmol, 2 equiv), capped with a rubber septum and evacuated. After backfilling with N<sub>2</sub>, this process was repeated three times. To the flask were added dry DMF (20 mL) and Et<sub>3</sub>N (20 mL) at room temperature. The reaction mixture was heated at 65 °C, and maintained under continuous stirring for 4 h, until the disappearance of compound **6** by TLC (Hexane/EtOAc 70:30). Solvents were removed under reduced pressure and the solid residue was dissolved in CH<sub>2</sub>Cl<sub>2</sub> and filtered on celite. The volatiles were removed *in vacuo* and the reaction crude was purified by flash chromatography on silica gel, using Hexane/EtOAc (90:10) as eluant, giving compound **8** as a pale yellow oil (0.91 g, 1.55 mmol, 60%). TLC: *R*<sub>f</sub> 0.60. <sup>1</sup>H NMR: δ 7.48 (d, *J*<sub>5,6</sub> = 8.1, 1H, H-5), 7.11 (d, *J*<sub>2,6</sub> = 1.0, 1H, H-2), 6.93 (dd, *J*<sub>5,6</sub> = 8.1, *J*<sub>2,6</sub> = 1.0, 1H, H-6), 5.25 (t, *J*<sub>2',3'</sub> = *J*<sub>3',4'</sub> = 9.3, 1H, H-3'), 5.10 (t, *J*<sub>3',4'</sub> = *J*<sub>4',5'</sub> = 9.3, 1H, H-4'), 5.02 (bdd, *J*<sub>1',2'</sub> = 8.3, *J*<sub>2',3'</sub> = 9.3, 1H, H-2'), 4.80 (d, *J*<sub>1',2'</sub> = 8.3, 1H, H-1'), 4.56 (s, 2H, CH<sub>2</sub>C≡), 4.27 and 4.14 (split AB system, *J*<sub>5',6A'</sub> = 4.2, *J*<sub>5',6B'</sub> = 1.8, *J*<sub>6A',6B'</sub> = 12.6, 2H, H<sub>2</sub>-6'), 3.79 (m, 1H, H-5'), 2.78 (s, 6H, [N(CH<sub>3</sub>)<sub>2</sub>]), 2.06, 2.03, 2.01 and 1.99 (four s,

12H, 4 × CH<sub>3</sub>CO). <sup>13</sup>C NMR: δ 170.6, 170.2 and 169.4 (4 × CO), 151.9 (C-3), 134.0 (C-5), 126.8 and 123.6 (C-2 and C-6), 121.9 and 119.9 (C-1 and C-4), 98.4 (C-1'), 86.3 and 83.9 (C≡C), 72.7 (C-3'), 71.8 (C-5'), 71.1 (C-2'), 68.2 (C-4'), 61.8 (C-6'), 56.8 (CH<sub>2</sub>C≡), 44.0 ([N(CH<sub>3</sub>)<sub>2</sub>]), 20.6 and 20.5 (4 × CH<sub>3</sub>CO). Calc. for C<sub>25</sub>H<sub>30</sub>BrNO<sub>10</sub> 583.11; found positive ESI-MS: [M-H<sup>+</sup>] = 584.1114.

#### 4.1.2. 3-[3-(Dimethylamino)-4-[2-(trimethylsilyl)ethynyl]phenyl]-2-propyn-1-yl-β-D-glucopyranoside-2,3,4,6-tetraacetate (**9**)

To a flask were added Pd(PPh<sub>3</sub>)<sub>4</sub> (0.27 g, 0.23 mmol, 0.15 equiv), **8** (0.91 g, 1.55 mmol, 1 equiv) and ethynyltrimethylsilane (1.31 mL, 9.3 mmol, 6 equiv), capped with a rubber septum and evacuated. After backfilling with N<sub>2</sub>, this process was repeated three times. To the flask were added dry DMF (11 mL) and Et<sub>3</sub>N (11 mL) at room temperature. The mixture was heated at 65 °C, and maintained under continuous stirring for 24 h, until the disappearance of compound **8** by TLC (Hexane/EtOAc 70:30). Solvents were removed *in vacuo* and the solid residue was dissolved in CH<sub>2</sub>Cl<sub>2</sub> and filtered on

and 2-based PDT. (**B**) Images correspond to cells treated with 3 · 10<sup>-6</sup> M of **1** or **2** followed by 0.25 J/cm<sup>2</sup> of UVA light (LD50 dose). PDT induced visible alterations in cell morphology. In the case of HaCaT cells, PDT using OPE-1 and OPE-2 triggered the appearance of apoptotic/necrotic cells. In HeLa and HEp-2 cells, in addition to apoptotic/necrotic figures, both treatments induced a large number of cells with rounded morphology (potential mitotic blockage) and cells detached from substrate. Scale bar: 30 μm.

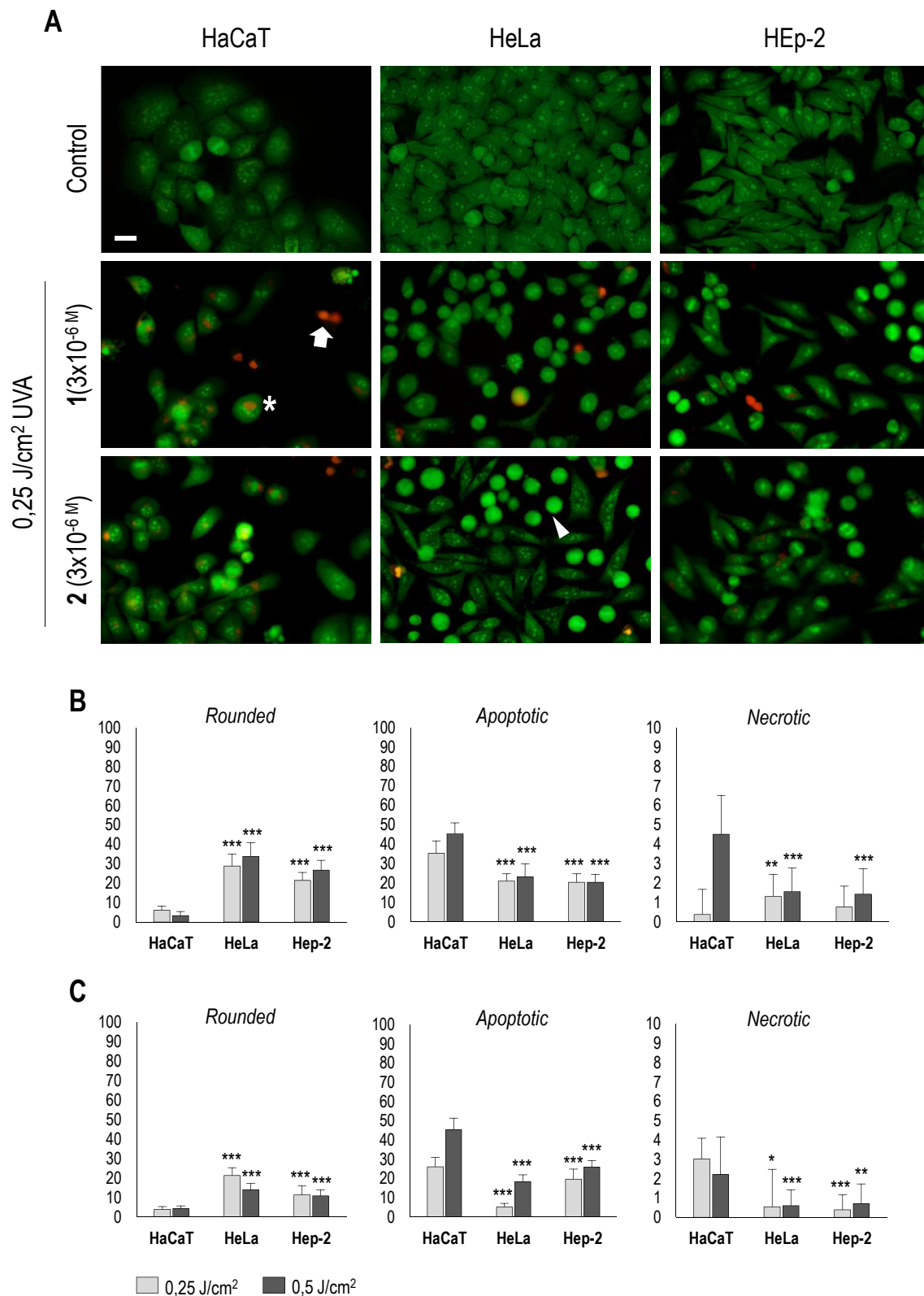


**Fig. 8.** AO/EtBr staining. **A:** HaCaT, HeLa and HEp-2 cells were *in vivo* stained with AO/EtBr 24 h after PDT with **1** and **2** in LD50 conditions. While untreated cells (control) showed a normal morphology, cells subjected to PDT presented morphological alterations, similar for both PSs. In the case of HaCaT cells, the treatments induced apoptotic (\*) and necrotic figures (arrow). In the tumoral cells (HeLa and HEp-2), in addition to apoptotic and necrotic cells, PDT triggered the appearance of a great number of cells with rounded morphology (arrowhead) (potential mitotic blockage). Scale bar: 20  $\mu$ m. **B–C:** Graphs show the percentages of rounded, apoptotic and necrotic cells 24 h after LD50 conditions of **1** (**B**) and **2** (**C**) mediated PDT. The number of cells with rounded morphology (possible mitotic arrest) were significantly increased in tumoral cells (HeLa and HEp-2) with respect to HaCaT cells. By contrast, the amount of apoptotic and necrotic morphologies was significantly higher in HaCaT than in HeLa and HEp-2 cells. \*: significant  $P < 0.1$ ; \*\*: significant  $P < 0.05$ ; \*\*\*: significant  $P < 0.01$ .

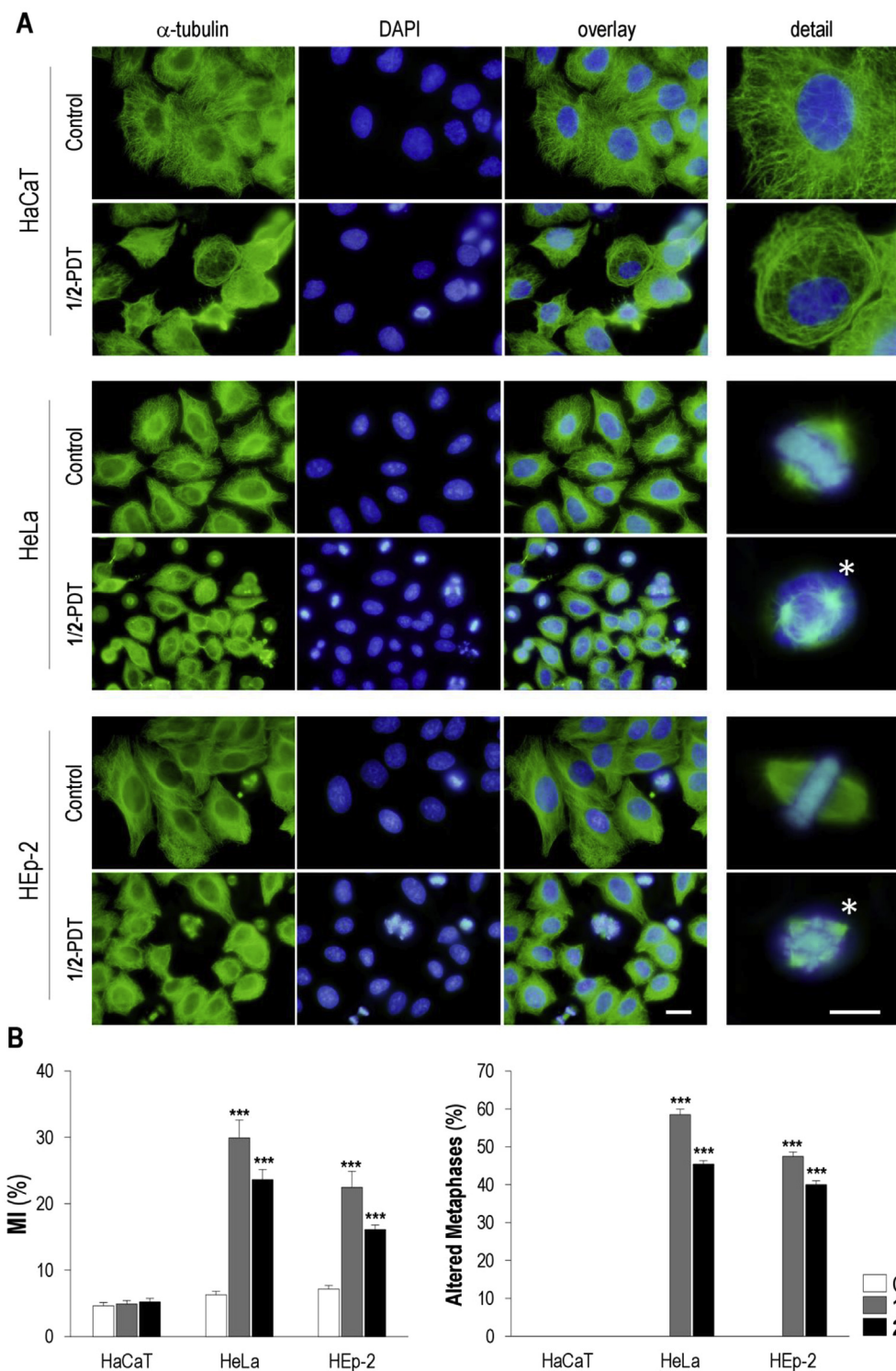


**Fig. 9.** Effects of OPE-1 or OPE-2 based PDT in microtubules from cytoskeleton (LD50 conditions). **A:** Microtubules from cytoskeleton of HaCaT, HeLa and HEp-2 cells were analyzed by immunofluorescence of  $\alpha$ -tubulin 24 h after **1** and **2**-PDT. Untreated (control) cells showed a well-developed MT network, while MTs of cells subjected to PDT appeared disorganized. In addition, the increased number of dividing cells in tumoral lines presented alterations in the mitotic apparatus and abnormalities in the distribution of chromosomes in the metaphase plate (\*). Scale bar: 10  $\mu$ m. **B:** Mitotic index and altered metaphases after **1** and **2**-based PDT.

celite. The volatiles were removed under vacuum and the crude purified by flash chromatography on silica gel using Hexane/EtOAc (90:10) as eluant to give compound **9** as a yellow oil (0.77 g, 1.27 mmol, 82%). TLC:  $R_f$  0.55.  $^1\text{H}$  NMR:  $\delta$  7.31 (d,  $J_{5,6} = 7.8$ , 1H, H-5), 6.86 (d,  $J_{2,6} = 1.2$ , 1H, H-2), 6.87 (dd,  $J_{5,6} = 7.8$ ,  $J_{2,6} = 1.2$ , 1H, H-6),

5.24 (t,  $J_{2,3'} = J_{3',4'} = 9.3$ , 1H, H-3'), 5.09 (t,  $J_{3',4'} = J_{4',5'} = 9.3$ , 1H, H-4'), 5.01 (bdd,  $J_{1',2'} = 8.1$ ,  $J_{2',3'} = 9.3$ , 1H, H-2'), 4.82 (d,  $J_{1',2'} = 8.1$ , 1H, H-1'), 4.57 (s, 2H,  $\text{CH}_2\text{C}\equiv$ ), 4.27 and 4.15 (split AB system,  $J_{5',6A'} = 4.5$ ,  $J_{5',6B'} = 2.1$ ,  $J_{6A',6B'} = 12.3$ , 2H, H<sub>2</sub>-6'), 3.74 (m, 1H, H-5'), 2.94 (s, 6H,  $[\text{N}(\text{CH}_3)_2]$ ), 2.06, 2.03, 2.01 and 1.99 (four s, 12H, 4  $\times$

CH<sub>3</sub>CO), 0.24 (s, 9H, [Si(CH<sub>3</sub>)<sub>3</sub>]), <sup>13</sup>C NMR: δ 170.6, 170.2, 169.4 and 169.3 (4 × CO), 154.8 (C-3), 134.8 (C-5), 123.2 and 119.8 (C-2 and C-6), 122.8 and 116.2 (C-1 and C-4), 104.0, 101.7, 87.2 and 84.4 (C≡C), 98.4 (C-1'), 72.8 (C-3'), 71.9 (C-5'), 71.1 (C-2'), 68.3 (C-4'), 61.8 (C-6'), 56.9 (CH<sub>2</sub>C≡), 43.1 [N(CH<sub>3</sub>)<sub>2</sub>], 21.0, 20.7 and 20.5 (4 × CH<sub>3</sub>CO), 0.2 ([Si(CH<sub>3</sub>)<sub>3</sub>]). Calc. for C<sub>30</sub>H<sub>39</sub>N<sub>10</sub>Si 601.23; found positive ESI-MS: [M-H<sup>+</sup>] = 602.2422.

#### 4.1.3. (2,5-Dimethoxy-1,4-phenylene)bis[2,1-ethynediyl[2-(dimethylamino)-4,1-phenylene]-2-propyne-3,1-diyl]-bis-β-D-glucopyranoside-2,2',3,3',4,4',6,6'-octaacetate (**10**)

To a flask were added Pd(PPh<sub>3</sub>)<sub>4</sub> (0.11 g, 0.09 mmol, 0.15 equiv), Ag<sub>2</sub>O (0.30 g, 1.28 mmol, 2 equiv), **9** (0.77 g, 1.28 mmol, 2 equiv) and 1,4-diiodo-2,5-dimethoxybenzene **5** (0.25 g, 0.64 mmol, 1 equiv), capped with a rubber septum and evacuated. After backfilling with N<sub>2</sub>, this process was repeated three times. To the flask were added dry DMF (10 mL) and dry THF (5 mL). The reaction mixture was heated at 70 °C for 7 h, until the disappearance of compound **9** by TLC (Hexane/EtOAc 50:50). Solvents were removed *in vacuo* and the solid residue was dissolved in CH<sub>2</sub>Cl<sub>2</sub> and filtered on celite. The volatiles were removed under reduced pressure and the crude purified by column chromatography on silica gel using Hexane/EtOAc (60:40) as eluant to give compound **10** as a brilliant yellow oil (0.43 g, 0.36 mmol, 57%). TLC: R<sub>f</sub> 0.35. <sup>1</sup>H NMR: δ 7.45 (d, J<sub>5',6'</sub> = 7.8, 2H, 2 × H-5'), 6.99 (s, 2H, H-3 and H-6), 6.97 (d, J<sub>2',6'</sub> = 1.2, 2H, 2 × H-2'), 6.96 (dd, J<sub>5',6'</sub> = 7.8, J<sub>2',6'</sub> = 1.2, 2H, 2 × H-6'), 5.28 (t, J<sub>2'',3''</sub> = J<sub>3'',4''</sub> = 9.3, 2H, 2 × H-3''), 5.12 (t, J<sub>3'',4''</sub> = J<sub>4'',5''</sub> = 9.3, 2H, 2 × H-4''), 5.04 (bdd, J<sub>1'',2''</sub> = 8.2, J<sub>2'',3''</sub> = 9.3, 2H, 2 × H-2''), 4.85 (d, J<sub>1'',2''</sub> = 8.2, 2H, 2 × H-1''), 4.60 (s, 4H, 2 × CH<sub>2</sub>C≡), 4.29 and 4.17 (split AB system, J<sub>5'',6A''</sub> = 4.4, J<sub>5'',6B''</sub> = 2.5, J<sub>6A'',6B''</sub> = 12.2, 4H, 2 × H<sub>2</sub>-6''), 3.89 (s, 6H, 2 × OCH<sub>3</sub>), 3.77 (m, 2H, 2 × H-5''), 3.03 (s, 12H, 2 × [N(CH<sub>3</sub>)<sub>2</sub>]), 2.08, 2.05, 2.03 and 2.02 (four s, 24H, 8 × CH<sub>3</sub>CO). <sup>13</sup>C NMR: δ 170.6, 170.2, 169.4 and 169.3 (8 × CO), 154.3 and 153.9 (C-2, C-5, C-3'), 134.3 (C-5'), 123.5 (C-6'), 122.6 (C-4'), 119.9 (C-2'), 115.5, 114.9 and 114.8 (C-1, C-3, C-4 and C-6), 113.6 (C-1'), 98.4 (C-1''), 98.1, 93.0, 87.2 and 84.4 (C≡C), 72.7 (C-3''), 71.8 (C-5''), 71.1 (C-2''), 68.3 (C-4''), 61.7 (C-6''), 56.9 (CH<sub>2</sub>C≡), 56.3 (OCH<sub>3</sub>), 43.3 [N(CH<sub>3</sub>)<sub>2</sub>], 20.7 and 20.5 (8 × CH<sub>3</sub>CO). Calc. for C<sub>62</sub>H<sub>68</sub>N<sub>2</sub>O<sub>22</sub> 1192.43; found positive MALDI [M<sup>+</sup>] = 1192.4; Purity by qNMR: 96.3%.

#### 4.1.4. (2,5-Dimethoxy-1,4-phenylene)bis[2,1-ethynediyl[2-(dimethylamino)-4,1-phenylene]-2-propyne-3,1-diyl]-bis-β-D-glucopyranoside (**2**)

To a flask was added **10** (0.43 g, 0.36 mmol) and dissolved in a mixture of MeOH (15 mL) and THF (15 mL). A large excess (9 mL) of aqueous ammonia was added to the obtained solution and the reaction was maintained under continuous stirring overnight at RT. Solvents were removed under reduced pressure and the undesired acetamide was eliminated by a series of MeOH washings, with the final obtaining of compound **2** as a brilliant yellow solid (0.30 g, 0.35 mmol, 97%). TLC: R<sub>f</sub> 0.05 (CHCl<sub>3</sub>/MeOH 80:20). Mp 123–125 °C. <sup>1</sup>H NMR (dmsO-d<sub>6</sub>): δ 7.40 (d, J<sub>5',6'</sub> = 8.7, 2H, 2 × H-5'), 7.12 (s, 2H, H-3 and H-6), 6.95 (m, 4H, 2 × H-2' and 2 × H-6'), 5.14 (d, J<sub>2'',OH</sub> = 4.4, 2H, 2 × OH-2''), 4.97 and 4.92 (two d, J<sub>3'',OH</sub> = J<sub>4'',OH</sub> = 4.4, 4H, 2 × OH-3'' and 2 × OH-4''), 4.64 and 4.51 (AB system and m, J<sub>gem</sub> = 15.7, 6H, 2 × CH<sub>2</sub>C≡ and 2 × OH-6''), 4.31 (d, 2H, J<sub>1'',2''</sub> = 7.8, 2 × H-1''), 3.83 (s, 6H, 2 × OCH<sub>3</sub>), 3.70 and 3.46 (split AB m, 4H, 2 × H<sub>2</sub>-6''), 3.16–2.98 (m, 8H, 2 × H-2'', 2 × H-3'', 2 × H-4'', 2 × H-5''), 2.96 (s, 12H, 2 × [N(CH<sub>3</sub>)<sub>2</sub>]). <sup>13</sup>C NMR (dmsO-d<sub>6</sub>): δ 153.9 and 153.5 (C-2, C-5 and C-3'), 134.4 (C-5'), 131.5 (C-1'), 122.8, 122.6, 119.5 and 119.4 (C-2' and C-6'), 114.9 and 114.8 (C-3 and C-6), 113.7 and 112.9 (C-1, C-4 and C-4'), 101.2 (C-1''), 94.2, 92.8, 87.1 and 85.6 (C≡C), 77.0 and 76.5 (C-3'' and C-5''), 73.3 (C-2''), 70.0 (C-4''), 61.3 (C-6''), 56.2 (CH<sub>2</sub>C≡), 55.7 (OCH<sub>3</sub>), 42.6 [N(CH<sub>3</sub>)<sub>2</sub>]. Calc. for C<sub>46</sub>H<sub>52</sub>N<sub>2</sub>O<sub>14</sub> 856.34; found positive ESI-MS: [M-H<sup>+</sup>] = 857.3515; Purity by qNMR: 96.3%.

## 4.2. Singlet oxygen evaluation

A direct comparison between the oligomers and Methylene blue species in solution by monitoring the UA photooxidation is not possible, because different excitation wavelengths were used for the photoproduction of <sup>1</sup>O<sub>2</sub>. Therefore, the efficiency of singlet-oxygen deliver was calculated by normalizing for the photon flux of the lamp at the lambda used for excitation (400 nm for OPEs and 600 nm for the methylene blue).

The absorption spectra were recorded in ultrapure spectroscopic solvents. UV/Vis absorption spectra were taken on a Jasco V-560 spectrophotometer. For steady-state luminescence measurements, a Jobin Yvon-Spex Fluoromax 2 spectrofluorimeter was used, equipped with a Hamamatsu R3896 photomultiplier. The spectra were corrected for photomultiplier response using software purchased with the fluorimeter. For the luminescence lifetimes, an Edinburgh OB 900 time-correlated single-photon-counting spectrometer was used. As excitation sources, a Hamamatsu PLP 2 laser diode (59 ps pulse width at 408 nm) and/or the nitrogen discharge (pulse width 2 ns at 337 nm) were employed. Emission quantum yields for acetonitrile deaerated solutions were determined using the optically diluted method [43]. As luminescence quantum yield standards we used an air equilibrated ethanol solution of anthracene (0.2) [44]. Experimental uncertainties on the absorption and photophysical data are as follows: absorption maxima, 2 nm; molar absorption, 15%; luminescence maxima, 4 nm; luminescence lifetimes, 10%; luminescence quantum yields, 20%.

## 5. Biological study. Materials and methods

### 5.1. Cell cultures

The human carcinoma cells used in this study were HEp-2 (derived from a larynx carcinoma) and HeLa (derived from a cervical carcinoma) cells. The spontaneously transformed HaCaT cell line, obtained from human keratinocytes, has been used as control of nontumorigenic cells. HeLa and HaCaT cells were cultured using Dulbecco's modified Eagle's medium (DMEM), supplemented with 10% (v/v) fetal bovine serum (FBS), 50 units/mL penicillin and 50 µg/mL streptomycin. HEp-2 cells were cultured in RPMI medium also supplemented with FBS, penicillin and streptomycin (all from GE Healthcare Life Sciences, HyClone Laboratories, Logan, Utah, USA). Cell cultures were performed under standard conditions at 37 °C, 95% of humidity and 5% of CO<sub>2</sub> and the medium was changed each two days.

### 5.2. Photosensitizers administration

Stock solutions of both **1** and **2** were prepared in DMSO (Pan-reac) at a concentration of 10<sup>-3</sup> M. The work solutions were obtained by dissolving the compounds in DMEM/RPMI with 1% FBS. The final concentration of DMSO was always lower than 0.5% (v/v), and the lack of toxicity of this solvent for the cells was also tested and confirmed. All the treatments were performed when cultures reached around 60–70% of confluence.

### 5.3. Intracellular localization of **1** and **2**

For the analysis of **1** and **2** subcellular localization, the cells were plated on glass coverslips placed into wells and incubated with 1 × 10<sup>-6</sup> M of **1** or **2** for 6 h at 37 °C. After incubation, cells were washed twice with PBS, mounted on slides with a drop of PBS and immediately observed under the fluorescence microscope coupled to a digital capture camera (Olympus BX61) using the appropriate filters of excitation light (UV, 365 nm, exciting filter UG-1). In

addition, to better determine the intracellular localization of **1** or **2**, the distribution pattern of both compounds was compared with that of specific organelles. For this purpose, cells were incubated with known fluorescent probes for endoplasmic reticulum (ER-Tracker, Molecular Probes; Eugene, OR) and Golgi apparatus (NBD, Molecular Probes; Eugene, OR). The fluorescent probes were used at the concentrations indicated by the suppliers and were incubated for 30 min. After incubation, cells were washed twice in PBS and observed under fluorescence microscope. The fluorescence excitation and emission wavelengths of ER-Tracker were 374 and 430 nm respectively. In the case of NBD were 466 and 536 nm respectively.

#### 5.4. Photodynamic treatments

Cells seeded on 24 well plates were incubated for 6 h with variable concentrations of **1** or **2** (from  $3 \cdot 10^{-6}$  M to  $2.5 \cdot 10^{-5}$  M). Afterwards, the media were removing, replaced by fresh media and cells were irradiated with different UVA light doses, ranging from 0.25 to 2 J/cm<sup>2</sup> (UVA source: CAMAG,  $\lambda = 300$ –400 nm, power: 15.9 W/m<sup>2</sup> at 10 cm from the source). After irradiation, cells were washed three times with PBS, complete DMEM or RPMI was added, and were maintained in the incubator for 24 h until evaluation. To assess the possible dark cytotoxic effect of both PSs, cells were incubated in the dark for 18 h with different PS concentrations. In the same way, to test the effect of UVA light alone, cells were subjected to different light doses (0.25–2 J/cm<sup>2</sup>).

#### 5.5. Morphological studies

Changes in general cell morphology and nuclear morphology after PDT were analyzed by phase contrast microscopy and Hoescht-33258 staining, respectively. In the second case, cells were fixed in formaldehyde (3.7% in PBS) for 15 min, washed and stained with 2.5  $\mu$ g/mL Hoescht-33258 dye (H-33258) (Sigma) for 5 min. After washing with distilled water, preparations were mounted with ProLong<sup>®</sup> Gold Antifade Reagent (Invitrogen). Death type was determinate analyzing nuclei morphology according to morphological criteria previously published [45].

#### 5.6. Viability assays

Cell viability was assessed 24 h after treatments using the MTT assay and the acridine orange (AO)/ethidium bromide (EtBr) method. Regarding the MTT assay, following treatments, 3-[4,5-dimethylthiazol-2-yl]-2,5-diphenyltetrazoliumbromide (MTT Sigma, St Louis, USA) solution was added to each well at a final concentration of 50  $\mu$ g/mL, and plates were incubated at 37 °C for 4 h. The formazan crystals were dissolved in DMSO and the absorbance at 542 nm was measured using a spectrophotometer (Espectra Fluor 4, Tecan). The results were expressed as cell survival percentage of control (cell survival (%)) = (mean OD value of PDT-treated cells/mean OD value of control cells) x 100%.

The AO/EB method was applied according as previously described by Liu and cols [46]. This method allowed us to confirm the tendency of the cell death rate detected by MTT assay and, moreover, to determine approximately the type of cell death induced by PDT. AO is a vital dye able to stain nuclear DNA across an intact cell membrane, while EB can only stains cells that have lost their membrane integrity. A solution of PBS containing 50  $\mu$ g/ml AO and 50  $\mu$ g/ml EB was prepared. Then, 300  $\mu$ L of this solution were added to each well and immediately analyzed under the fluorescence microscope. 200 cells of each condition were counted within 15 min after the addition of the fluorochromes. Cells were classified as (1) living cells (uniformly stained as green), (2) rounded cells

(possible mitotic arrest and densely stained as green); (3) apoptotic cells (early apoptosis: densely stained as green but showing orange fragments; late apoptosis: densely stained as orange and condensed chromatin) and (4) necrotic cells (uniformly stained as orange-red stained and no chromatin condensation) (Fig. S17, ESI).

#### 5.7. Immunofluorescence

For immunodetection of  $\alpha$ -tubulin, cells were raised on coverslips and subjected to PDT and, 24 h after treatment, were fixed and permeabilized in methanol ( $-20$  °C) for 7 min. Then, cells were washed twice in PBS and incubated with  $\alpha$ -tubulin primary antibody (Sigma-Aldrich, St. Louis, MO) for 1 h at 37 °C. After washing, cells were incubated with Alexa Fluor 488-conjugated goat anti-mouse IgG secondary antibody (1:250) (Invitrogen, California, USA) for 45 min at 37 °C, washed in PBS and mounted in Prolong Gold Antifade Reagent (Invitrogen, California, USA).

#### 5.8. Microscopical observations and statistical analysis

Microscopic observation was carried out using a fluorescence microscope (Olympus BX61) equipped with the following filter sets for fluorescence microscopy: ultraviolet (UV, 365 nm, exciting filter UG-1), blue (450–490 nm, exciting filter BP 490), and green (545 nm, exciting filter BP 545). Images were obtained with the digital camera Olympus CCD DP70 and processed using the Adobe PhotoShop CS5 extended version 12.0 software (Adobe Systems Inc., USA).

Data are expressed as the mean value  $\pm$  standard deviations (SD). Statistical analysis was carried out with SPSS Statistics 20.0 (IBM<sup>®</sup>). The statistical significance was determined using the T test for independent samples (\*:  $P < 0.1$ ; \*\*:  $P < 0.05$ ; \*\*\*:  $P < 0.01$ ).

#### Acknowledgment

We thank Prof. Anna Notti for the very helpful discussion on qNMR analyses. We thank MIUR, Italy (PRIN 20109Z2XRJ\_010), Spanish MINECO grant FIS PI12/01253, CTQ2011-24783, CTQ2014-53894-R and Comunidad Autónoma de Madrid grant SkinModel CAM S10/BMD-2359.

#### Appendix A. Supplementary data

Supplementary data related to this article can be found at <http://dx.doi.org/10.1016/j.ejmech.2016.01.041>

#### References

- [1] P. Agostinis, K. Berg, K.A. Cengel, T.H. Foster, A.W. Girotti, S.O. Gollnick, S.M. Hahn, M.R. Hamblin, A. Juzeniene, D. Kessel, M. Korbelik, J. Moan, P. Mroz, D. Nowis, J. Piette, B.C. Wilson, J. Golab, Photodynamic therapy of cancer: an update, *CA. Cancer. J. Clin.* 61 (2011) 250–281.
- [2] M.T. Wan, J.Y. Lin, Current evidence and applications of photodynamic therapy in dermatology, *Clin. Cosmet. Investig. Dermatol.* 7 (2014) 145–163.
- [3] F. Almutawa, L. Thalib, D. Hekman, Q. Sun, I. Hamzavi, H.W. Lim, Efficacy of localized phototherapy and photodynamic therapy for Psoriasis: a systematic review and meta-analysis, *Photodermatol. Photoimmunol. Photomed.* 31 (2015) 5–14.
- [4] M. Situm, V. Bulat, K. Majcen, A. Dzapo, J. Jezovita, Benefits of controlled ultraviolet radiation in the treatment of dermatological diseases, *Coll. Antropol.* 38 (2014) 1249–1253.
- [5] J.O. Yoo, K.S. Ha, New insights into the mechanisms for photodynamic therapy-induced cancer cell death, *Int. Rev. Cell. Mol. Biol.* 295 (2012) 139–174.
- [6] V.V. Serra, A. Zamarrón, M.A.F. Faustino, M.C.I. Cruz, A. Blázquez, J.M.M. Rodrigues, M.G.P.M.S. Neves, J.A.S. Cavaleiro, A. Juarranz, F. Sanz-Rodríguez, New porphyrin amino acid conjugates: synthesis and photodynamic effect in human epithelial cells, *Bioorg. Med. Chem.* 18 (2010) 6170–6178.
- [7] S. Dogra, R. Mahajan, Phototherapy for mycosis fungoides, *Indian. J. Dermatol.*

- Venereol. Leprol. 81 (2015) 124–135.
- [8] A. Pérez-Ferriols, B. Aranegui, J.A. Pujol-Montcusí, A. Martín-Gorgojo, M. Campos-Domínguez, R.A. Feltes, Y. Gilaberte, B. Echeverría-García, A. Alvarez-Pérez, I. García-Doval, Phototherapy in atopic dermatitis: a systematic review of the literature, *Actas Dermosifiliogr.* 106 (2015) 387–401.
- [9] E. Racz, E.P. Prens, Phototherapy and photochemotherapy for psoriasis, *Dermatol. Clin.* 33 (2015) 79–89.
- [10] A.R.M. Soares, M.G.P.M.S. Neves, A.C. Tome, M.C. Iglesias-de la Cruz, A. Zamarrón, E. Carrasco, S. González, J.A.S. Cavaleiro, T. Torres, D.M. Guldi, R.R. Allison, Glycophthalocyanines as photosensitizers for triggering mitotic catastrophe and apoptosis in cancer cells, *Chem. Res. Toxicol.* 25 (2012) 940–951.
- [11] U. Basu, I. Khan, A. Hussain, B. Gole, P. Kondaiah, A.R. Chakravarty, Carbohydrate-appended tumor targeting iron(III) complexes showing photocytotoxicity in red light, *Inorg. Chem.* 53 (2014) 2152–2162.
- [12] R.R. Allison, G.H. Downie, R. Cuenca, X.H. Hu, C.J.H. Childs, C.H. Sibata, Photosensitizers in clinical PDT, *Photodiagn. Photodyn. Ther.* 1 (2004) 27–42.
- [13] M.J. Garland, C.M. Cassidy, D. Woolfson, R.F. Donnelly, Designing photosensitizers for photodynamic therapy: strategies, challenges and promising developments, *Future Med. Chem.* 1 (2009) 667–691.
- [14] Y. Yamaguchi, T. Tanaka, S. Kobayashi, T. Wakamiya, Y. Matsubara, Z.-i. Yoshida, Light-emitting efficiency tuning of Rod-shaped  $\pi$  conjugated systems by donor and acceptor groups, *J. Am. Chem. Soc.* 127 (2005) 9332–9333.
- [15] E.H. Hill, H.C. Pappas, D.G. Evans, D.G. Whitten, Cationic oligo-*p*-phenylene ethynylenes form complexes with surfactants for long-term light-activated biocidal applications, *Photochem. Photobiol. Sci.* 13 (2014) 247–253.
- [16] F. Pertici, N. Varga, A. van Duijn, M. Rey-Carrizo, A. Bernardi, R.J. Pieters, Efficient synthesis of phenylene-ethynylene rods and their use as rigid spacers in divalent inhibitors, *Beilstein J. Org. Chem.* 9 (2013) 215–222.
- [17] Y.-G. Zhi, S.-W. Lai, Q.K.-W. Chan, Y.-C. Law, G.S.-M. Tong, C.-M. Che, Systematic studies on photoluminescence of oligo(arylene-ethynylene)s: tunability of excited states and derivatization as luminescent labeling probes for proteins, *Eur. J. Org. Chem.* (2006) 3125–3139.
- [18] A. Cardone, F. Lopez, F. Affortunato, G. Busco, A.M. Hofer, R. Mallamaci, C. Martinelli, M. Colella, G.M. Farinola, An aryleneethynylene fluorophore for cell membrane staining, *Biochim. Biophys. Acta* 1818 (2012) 2808–2817.
- [19] T. Papalia, G. Siracusano, I. Colao, A. Barattucci, M.C. Aversa, S. Serroni, G. Zappalà, S. Campagna, M.T. Sciortino, F. Puntoriero, P. Bonaccorsi, Cell internalization of BODIPY-based fluorescent dyes bearing carbohydrate residues, *Dyes Pigments* 110 (2014) 67–71.
- [20] P. Bonaccorsi, M.C. Aversa, A. Barattucci, T. Papalia, F. Puntoriero, S. Campagna, Artificial light-harvesting antenna systems grafted on a carbohydrate platform, *Chem. Commun.* 48 (2012) 10550–10552.
- [21] P. Bonaccorsi, F. Marino-Merlo, A. Barattucci, G. Battaglia, E. Papaiani, T. Papalia, M.C. Aversa, A. Mastino, Synthesis and biological evaluation of a new class of glycoconjugated disulfides that exhibit potential anticancer properties, *Bioorg. Med. Chem.* 20 (2012) 3186–3195.
- [22] A. Barattucci, E. Deni, P. Bonaccorsi, M.G. Ceraolo, T. Papalia, A. Santoro, M.T. Sciortino, F. Puntoriero, Oligo(phenylene-ethynylene) glucosides: modulation of cellular uptake capacity preserving light ON, *J. Org. Chem.* 79 (2014) 5113–5120.
- [23] C. Granchi, F. Minutolo, Anticancer agents that counteract tumor glycolysis, *ChemMedChem* 7 (2012) 1318–1350.
- [24] C. Yi, C. Blum, M. Lehmann, S. Keller, S.-X. Liu, G. Frei, A. Neels, J. Hauser, S. Schürch, S.S. Decurtins, Versatile strategy to access fully functionalized benzodifurans: redox-active chromophores for the construction of extended  $\pi$ -conjugated materials, *J. Org. Chem.* 75 (2010) 3350–3357.
- [25] G.B. Giovenzana, L. Lay, D. Monti, G. Palmisano, L. Panza, Synthesis of carboranyl derivatives of alkynyl glycosides as potential BNCT agents, *Tetrahedron* 55 (1999) 14123–14136.
- [26] A. Mori, T. Kondo, T. Kato, Y. Nishihara, Palladium-catalyzed cross-coupling polycondensation of bisalkynes with dihaloarenes activated by tetrabutylammonium hydroxide or silver (I) oxide, *Chem. Lett.* (2001) 286–287.
- [27] F. Babudri, D. Colangiuli, P.A. Di Lorenzo, G.M. Farinola, O. Hassan Omar, F. Naso, Synthesis of poly(aryleneethynylene)s bearing glucose units as substituents, *Chem. Commun.* (2003) 130–131.
- [28] W.E. Parham, R.M. Piccirilli, Selective halogen-lithium exchange in 2,5-dibromobenzenes and 2,5-dibromopyridine, *J. Org. Chem.* 42 (1977) 257–260.
- [29] The structure of regioisomer 8 was unequivocally established by NMR, including HMBC experiments: see supporting information (ESI) for details.
- [30] P.-H. Lanoë, T. Gallavardin, A. Dupin, O. Maury, P.L. Baldeck, M. Lindgren, C. Monnerau, C. Andraud, Influence of bromine substitution pattern on the singlet oxygen generation efficiency of two-photon absorbing chromophores, *Org. Biomol. Chem.* 10 (2012) 6275–6278.
- [31] A. Passarella Gerola, J. Semensato, D. Silva Pellosi, V. Roberto Batistela, B. Ribeiro Rabello, N. Hioka, W. Caetano, Chemical determination of singlet oxygen from photosensitizers illuminated with LED: new calculation methodology considering the influence of photobleaching, *J. Photochem. Photobiol. A* 232 (2012) 14–21.
- [32] B. Ribeiro Rabello, A. Passarella Gerola, D. Silva Pellosi, A.L. Tessaro, J.L. Aparício, W. Caetano, N. Hioka, Singlet oxygen dosimetry using uric acid as a chemical probe: systematic evaluation, *J. Photochem. Photobiol. A* 238 (2012) 53–62.
- [33] A.P. Castano, T.N. Demidova, M.R. Hamblin, Mechanisms in photodynamic therapy: part three—photosensitizer pharmacokinetics, biodistribution, tumor localization and modes of tumor destruction, *Photodiagn. Photodyn. Ther.* 2 (2005) 91–106.
- [34] D. Kessel, Subcellular targets for photodynamic therapy: implications for initiation of apoptosis and autophagy, *J. Natl. Compr. Canc. Netw.* 10 (2012) 56–59.
- [35] A. Juarranz, P. Jaén, F. Sanz-Rodríguez, J. Cuevas, S. González, Photodynamic therapy of cancer. Basic principles and applications, *Clin. Transl. Oncol.* 10 (2008) 148–154.
- [36] R. Hornung, M.K. Fehr, H. Walt, P. Wyss, M.W. Berns, Y. Tadir, PEG-m-THPC-mediated photodynamic effects on normal rat tissues, *Photochem. Photobiol.* 72 (2000) 696–700.
- [37] F. Ricchelli, L. Franchi, G. Miotto, L. Borsetto, S. Gobbo, P. Nikolov, J.C. Bommer, E. Reddi, Meso-substituted tetra-cationic porphyrins photosensitize the death of human fibrosarcoma cells via lysosomal targeting, *Int. J. Biochem. Cell. Biol.* 37 (2005) 306–319.
- [38] A. Bernd, Visible light and/or UVA offer a strong amplification of the anti-tumor effect of curcumin, *Phytochem. Rev.* 13 (2014) 183–189.
- [39] A. Bernd, S. Simon, A. Ramirez Bosca, S. Kippenberger, J. Diaz Alperi, J. Miquel, J.F. Villalba Garcia, D. Pamies Mira, R. Kaufmann, Phototoxic effects of hypericum extract in cultures of human keratinocytes compared with those of psoralen, *Photochem. Photobiol.* 69 (1999) 218–221.
- [40] S. Rello-Varona, A. Gámez, V. Moreno, J.C. Stockert, J. Cristóbal, M. Pacheco, M. Cañete, A. Juarranz, A. Villanueva, Metaphase arrest and cell DEATH INDUCED by etoposide on HeLa cells, *Int. J. Biochem. Cell. Biol.* 38 (2006) 2183–2195.
- [41] J.F. Barata, A. Zamarrón, M.G. Neves, M.A. Faustino, A.C. Tomé, J.A. Cavaleiro, B. Röder, A. Juarranz, F. Sanz-Rodríguez, Photodynamic effects induced by meso-tris(pentafluorophenyl)corrole and its cyclodextrin conjugates on cytoskeletal components of HeLa cells, *Eur. J. Med. Chem.* 92 (2015) 135–144.
- [42] T.J. Henderson, Quantitative NMR spectroscopy using coaxial inserts containing a reference standard: purity determinations for military nerve agents, *Anal. Chem.* 74 (2002) 191–198.
- [43] N. Demas, G.A. Crosby, The measurement of photoluminescence quantum yields. A review, *J. Phys. Chem.* 75 (1971) 991–1024.
- [44] D.N. Dempster, T. Morrow, M.F. Quinn, Extinction coefficients for triplet-triplet absorption in ethanol solutions of anthracene, naphthalene, 2,5-diphenyloxazole, 7-diethylamino-4-methyl coumarin and 4-methyl-7-amino-carbostyryl, *J. Photochem.* 2 (1974) 329–341.
- [45] S. Rello, J.C. Stockert, V. Moreno, A. Gámez, M. Pacheco, A. Juarranz, M. Cañete, A. Villanueva, Morphological criteria to distinguish cell death induced by apoptotic and necrotic treatments, *Apoptosis* 10 (2005) 201–208.
- [46] K. Liu, P.C. Liu, R. Liu, X. Wu, Med. Dual AO/EB staining to detect apoptosis in osteosarcoma cells compared with flow cytometry, *Sci. Monit. Basic. Res.* 21 (2015) 15–20.